NeuroImage: Clinical 3 (2013) 132–142

Contents lists available at ScienceDirect

NeuroImage: Clinical

journal homepage: www.elsevier.com/locate/ynicl

Disrupted cerebral metabolite levels and lower nadir CD4+ counts are linked to brain volume deficits in 210 HIV-infected patients on stable treatment☆

Xue Hua [a], Christina P. Boyle [a], Jaroslaw Harezlak [b], David F. Tate [c], Constantin T. Yiannoutsos [b], Ron Cohen [d,e], Giovanni Schifitto [f], Assawin Gongvatana [e], Jianhui Zhong [g], Tong Zhu [g], Michael J. Taylor [h], Thomas B. Campbell [i], Eric S. Daar [j], Jeffry R. Alger [k], Elyse Singer [k], Steve Buchthal [l], Arthur W. Toga [a], Bradford Navia [m], Paul M. Thompson [a,*], the HIV Neuroimaging Consortium

[a] Imaging Genetics Center, Laboratory of Neuro Imaging, Dept. of Neurology, UCLA School of Medicine, Los Angeles, CA, USA
[b] Indiana University Fairbanks School of Public Health, Indianapolis, IN, USA
[c] Henry M. Jackson Foundation for the Advancement of Military Medicine Contractor, San Antonio Military Medical Center, San Antonio, TX, USA
[d] Centers for Behavioral and Preventive Medicine, The Miriam Hospital, Providence, RI, USA
[e] Department of Psychiatry and Human Behavior, the Warren Alpert Medical School of Brown University, Providence, RI, USA
[f] Department of Neurology, University of Rochester, Rochester, NY, USA
[g] Department of Imaging Sciences, University of Rochester, Rochester, NY, USA
[h] Department of Psychiatry, University of California, San Diego, CA, USA
[i] University of Colorado Denver, Aurora, CO, USA
[j] Los Angeles Biomedical Research Institute at Harbor-UCLA Medical Center, University of California, Los Angeles, CA, USA
[k] David Geffen School of Medicine at UCLA, Los Angeles, CA, USA
[l] Department of Medicine, JABSOM, University of Hawaii, Honolulu, HI, USA
[m] Department of Public Health, Infection Unit, Tufts University School of Medicine, Boston, MA, USA

ARTICLE INFO

Article history:
Received 17 May 2013
Received in revised form 3 July 2013
Accepted 25 July 2013
Available online xxxx

Keywords:
Combined antiretroviral therapy
HIV
Magnetic resonance imaging
Proton magnetic resonance spectroscopy
Tensor-based morphometry
Nadir CD4+

ABSTRACT

Cognitive impairment and brain injury are common in people with HIV/AIDS, even when viral replication is effectively suppressed with combined antiretroviral therapies (cART). Metabolic and structural abnormalities may promote cognitive decline, but we know little about how these measures relate in people on stable cART. Here we used tensor-based morphometry (TBM) to reveal the 3D profile of regional brain volume variations in 210 HIV+ patients scanned with whole-brain MRI at 1.5 T (mean age: 48.6 ± 8.4 years; all receiving cART). We identified brain regions where the degree of atrophy was related to HIV clinical measures and cerebral metabolite levels assessed with magnetic resonance spectroscopy (MRS). Regional brain volume reduction was linked to lower nadir CD4+ count, with a 1–2% white matter volume reduction for each 25-point reduction in nadir CD4+. Even so, brain volume measured by TBM showed no detectable association with current CD4+ count, AIDS Dementia Complex (ADC) stage, HIV RNA load in plasma or cerebrospinal fluid (CSF), duration of HIV infection, antiretroviral CNS penetration-effectiveness (CPE) scores, or years on cART, after controlling for demographic factors, and for multiple comparisons. Elevated glutamate and glutamine (Glx) and lower *N*-acetylaspartate (NAA) in the frontal white matter, basal ganglia, and mid frontal cortex — were associated with lower white matter, putamen and thalamus volumes, and ventricular and CSF space expansion. Reductions in brain volumes in the setting of chronic and stable disease are strongly linked to a history of immunosuppression, suggesting that delays in initiating cART may result in imminent and irreversible brain damage.

1. Introduction

Since the introduction of combined antiretroviral therapies (cART), opportunistic infections and HIV-associated dementia are much less common, resulting in marked improvements in life expectancy and quality of life for people living with HIV (Antinori et al., 2007; Palella et al., 1998; Schouten et al., 2011). Even so, the incidence of mild to moderate cognitive dysfunction is increasing in HIV+ cohorts (Ances

* Corresponding author at: Imaging Genetics Center, Laboratory of Neuro Imaging, Dept. of Neurology, UCLA School of Medicine, Neuroscience Research Building 225E, 635 Charles Young Drive, Los Angeles, CA 90095-1769, USA. Tel.: +1 310 206 2101; fax: +1 310 206 5518.
E-mail address: thompson@loni.ucla.edu (P.M. Thompson).

2213-1582/$ – see front matter © 2013 The Authors. Published by Elsevier Inc. All rights reserved.
http://dx.doi.org/10.1016/j.nicl.2013.07.009

and Ellis, 2007; Heaton et al., 2010, 2011). 15–50% of patients who have received long-term treatment show some cognitive impairment (Cysique et al., 2004; Simioni et al., 2010), suggesting continued central nervous system (CNS) involvement despite viral suppression and immune reconstitution.

Neuroimaging studies have provided useful insights into the pattern and extent of CNS damage associated with HIV infection (Jernigan et al., 1993; Tucker et al., 2004). The HIV Neuroimaging Consortium (HIVNC) was formed in 2005 to map the course of structural brain injury over time, and to relate brain changes to cognitive impairment in a prospective cohort of HIV+ subjects with a history of chronic disease on stable cART. Multimodal neuroimaging data was collected to assess the HIV+ brain in terms of: (1) cellular injury and inflammatory response measured by proton magnetic resonance spectroscopy (^{1}H-MRS) (Cohen et al., 2010a; Harezlak et al., 2011), and (2) structural brain atrophy measured from standard anatomical magnetic resonance imaging (MRI) (Cohen et al., 2010a, 2010b).

To date, neuroimaging studies of HIV+ populations have found important associations between CNS structural abnormalities, immunological markers, and neural injury reflected by brain metabolite disruption. Reduced cortical and subcortical volumes in addition to metabolite abnormalities persist in HIV patients receiving cART, and are associated with advanced disease stage and cognitive impairment (Chiang et al., 2007; Cohen et al., 2010a, 2010b; Harezlak et al., 2011; Patel et al., 2003; Paul et al., 2002, 2008; Tate et al., 2009, 2011). Among structural brain abnormalities, atrophy in the basal ganglia and frontal white matter, as well as abnormalities in periventricular white matter are most commonly observed, suggesting a primary involvement of the frontal–striatal networks (Dal Pan et al., 1992; Navia et al., 1986a; Tate et al., 2009). White matter atrophy is common in both pre- and post-cART HIV+ cohorts and is strongly associated with disturbances in cognitive function (Gongvatana et al., 2009; Navia et al., 1986a; Schouten et al., 2011). Abnormalities previously reported in the basal ganglia structures include either hypertrophy (an increase in volume) (Castelo et al., 2007) or hypotrophy (a deficit in volume) (Jernigan et al., 2005) in HIV+ patients, possibly due to the different stages of infection and response to treatment. Methamphetamine use may also cause hypertrophy of the white matter (perhaps due to inflammation); although the cause and consistency of the white matter effects of meth are not well-understood, some cohorts deliberately assess HIV participants with co-morbid IV drug use, where the balance of effects tends to reflect a combination of viral effects and those of chronic drug use. Recent evidence for white matter changes in HIV+ participants includes faster rates of white matter volume loss in HIV+ patients on stable cART with viral suppression (Cardenas et al., 2009), lower white matter fractional anisotropy as well as greater brain network deficits measured by diffusion tensor imaging (Chen et al., 2009; Jahanshad et al., 2012; Nir et al., 2013; Pfefferbaum et al., 2007; Pfefferbaum et al., 2009; Ragin et al., 2004; Tate et al., 2010; Wu et al., 2006). In the HIVNC cohort and a separate cohort named CNS HIV Antiretroviral Therapy Effects Research (CHARTER), nadir CD4+ count has been associated with lower total white matter and subcortical gray matter volumes (Cohen et al., 2010b; Jernigan et al., 2011), as well as lower corpus callosum volumes (Tate et al., 2011).

Brain MRS shows regional metabolite disturbances, including increases in choline and myoinistol, along with decreases in N-acetyl aspartate, reflecting inflammation and neuronal injury, respectively, in the frontal white matter and subcortical nuclei (Chang et al., 2004; Harezlak et al., 2011; Sacktor et al., 2005; Yiannoutsos et al., 2004). A recent HIVNC study of 240 HIV+ patients showed a persistence of these abnormalities in the setting of stable disease and cART (Harezlak et al., 2011). Although cerebral metabolite abnormalities were associated with cortical and subcortical gray matter deficits in the HIVNC cohort, significant relationships with white matter volume have not yet been detected (Cohen et al., 2010a). Here we set out to use a sensitive MRI analysis technique called tensor-based morphometry (TBM) to relate clinical markers of HIV infection and brain metabolites to differences in regional brain volume. TBM is a nonlinear registration based approach designed to detect regional differences in brain volume in a cohort, and study factors that affect them (Chiang et al., 2007; Chung et al., 2001; Davatzikos, 1996; Fox et al., 2001; Hua et al., 2013; Shen and Davatzikos, 2003; Studholme et al., 2001; Thompson et al., 2000). Multivariate TBM has been recently applied to study structural abnormalities (Lepore et al., 2008) and lateral ventricular surface differences (Wang et al., 2010) associated with HIV/AIDS. Unlike traditional ROI-based volumetric methods, TBM provides a whole brain voxel-based analysis without requiring any prior anatomical hypothesis about where differences should be found. It is a helpful method to study the profile of white matter atrophy on anatomical MRI, which lacks detectable anatomical landmarks to parcellate white matter in a consistent way.

Here we mapped the 3D pattern of brain abnormalities in a large cohort of HIV-infected patients on stable cART, as part of the HIVNC study. Regional brain volume variations in 210 HIV-infected patients – both cognitively asymptomatic and symptomatic – were examined for relationships with MRS cerebral metabolite levels and HIV clinical indices such as nadir and current CD4+ levels, HIV RNA concentrations and duration of known HIV infection. We hypothesized that the level of atrophy in frontal brain regions, particularly the white matter, and the basal ganglia, would relate to metabolic markers of neuronal injury, and to nadir CD4+ count, a marker of immune function and a major risk factor for neurocognitive impairment (Heaton et al., 2011).

2. Materials and methods

2.1. Subjects

We studied 210 HIV-infected patients (mean age 48.6 ± 8.4 years; 175 men and 35 women) enrolled in the HIVNC during the years 2003–2009. Subjects were recruited from seven sites across the United States including Colorado (N = 36), UCLA (N = 42), UCLA-Harbor (N = 54), UCSD (N = 11), Rochester (N = 49), Stanford (N = 15), and Pittsburgh (N = 3). Subjects of various ethnicities were enrolled, including Caucasians (N = 148; 70% of the cohort), African-Americans (N = 54; 26%), Asians (N = 2; 1%) and Native Americans and American Indians (N = 6; 3%). Inclusion criteria included nadir CD4+ cell count less than 200 cells/mm^3; stable antiretroviral regimen with any Food and Drug Administration (FDA)-approved therapy for at least 12 consecutive weeks prior to the study; hemoglobin greater than 9.0 g/dl; serum creatinine less than three times the upper limit of normal (ULN); aspartate aminotransferase (serum glutamic-oxaloacetic transaminase) [AST (SGOT)], alanine transaminase (serum glutamic–pyruvic transaminase) [ALT (SGPT)], and alkaline phosphatase of three times the ULN or less.

Exclusion criteria included severe premorbid or comorbid psychiatric disorders, confounding neurologic disorders such as chronic seizures, stroke, head trauma resulting in loss of consciousness of more than 30 min, multiple sclerosis, brain infection (except for HIV), or brain neoplasms, including CNS lymphoma and active alcohol and drug abuse or related medical complications within 6 months of study. All procedures were reviewed and approved by local institutional review boards (IRBs). All participants gave written informed consent.

2.2. Clinical characteristics

Clinical measures included the AIDS Dementia Complex (ADC) stage (Navia et al., 1986a, 1986b; Price and Brew, 1988), current CD4+ counts, nadir CD4+ counts (lowest cell counts prior to treatment), HIV RNA viral load in plasma and cerebrospinal fluid (CSF), duration of HIV infection or duration of known infection when patient was first tested, antiretroviral CNS penetration-effectiveness (CPE) scores, and years on cART. Although 210 participants were available for study,

certain clinical measures were only available in a subset of the sample (Table 1, Total N).

Global cognitive status was assessed using ADC staging, as previously described (Price and Brew, 1988). ADC staging is strongly correlated with the severity of brain pathology (Navia et al., 1986b), immunopathology (Brew et al., 1995) and abnormal brain metabolites (Chang et al., 1999) and provides a robust measure of cognitive function in HIV+ patients. ADC staging was performed by a trained clinician at each site based on the neurological examination, assessment of functional impairment, and neuropsychological performance, as previously described (Price et al., 1990). Neuropsychological impairment was defined as performance at least 1.0 standard deviation below normative values on two or more neuropsychological tests, or at least 2.0 standard deviations below normative values on one or more tests. Participants were classified as stage 0 (normal), 0.5 (subclinical), 1 (mild), 2 (moderate), 3 (severe), or 4 (end stage). In our study, 200 patients had ADC staging measures and no patients were at ADC stage 3 or 4 (Table 1). To summarize effects at different stages, we also converted the original ADC stage into a binary version (i.e., the "binary ADC stage"), with ADC stages 0 and 0.5 coded as "0" and ADC stages 1 and 2 coded as "1".

CD4+ counts and HIV RNA viral load were measured from each patient's blood sample (plasma) and CSF, using standardized methods (e.g., Roche Amplicor techniques) (Mulder et al., 1994). Pre-treatment CD4+ count or nadir CD4+ count is the most well known risk factor for, and predictor of, treatment outcomes and neurocognitive impairment in HIV infection (Schouten et al., 2011). It reflects the lowest measured cell count during the course of infection, indicating the severity of immunosuppression prior to the initiation antiretroviral therapy. The record of nadir CD4+ was obtained from the patient's medical history. Duration of HIV known infection (in years) was estimated as the time difference between the date of diagnosis of HIV seropositivity from the date of the image acquisition, and it should be understood that this does not necessarily reflect true duration of infection. The CPE scoring was based on the first proposal of Scott Letendre and colleagues (Letendre et al., 2009). CPE scores range from 0 to 4, with 87% of observations between 0.5 and 2.5.

2.3. Structural magnetic resonance imaging (MRI)

Each participant underwent a MRI scan using a 1.5 T scanner manufactured by GE Healthcare or Siemens Healthcare. GE scans followed a standardized structural imaging protocol that included a spoiled gradient-recalled echo (SPGR) T1-weighted volumetric scan with the following parameters: repetition time (TR) ranged from 20 to 22 ms; echo time (TE) ranged from 5 to 7 ms; field-of-view (FOV) = 20 cm; slice thickness = 1.3 mm; flip angle = 30°; matrix size = 256 × 128, with the number of excitations (NEX) set to 1. Siemens scans were performed on Sonata or Symphony models. Fourteen percent of the total scans (N = 29) were acquired on Siemens scanners. For scans performed with Siemens scanners we used a structural imaging pulse sequence and parameters matched to the protocol used on GE scanners (TR/TE of 20/10.1 ms; FOV = 22 cm; slice thickness = 1.3 mm; flip angle = 30°; matrix size = 256 × 192; NEX set to 1). Reliability and validity tests were conducted by imaging five subjects using the GE and Siemens scanners on the same day. Volumetric measures of a group of brain structures were made using FreeSurfer software on the 10 structural images from these five subjects. Volume differences attributable to scanner type were less than 5%. Accordingly, we did not perform separate TBM analyses for scans acquired with GE and Siemens scanners. Furthermore the small fraction of the scans done with Siemens scanners (14%) made it unlikely that any valid conclusions about scanner type bias could be drawn. But more importantly, there were no statistically significant differences in age, sex, or ethnicity (all p-values > 0.05) between the groups of subjects scanned on each scanner.

Table 1
Clinical characteristics of the study participants. Cognitive impairment was evaluated in 200 subjects, using AIDS dementia complex (ADC) scores. Median and interquartile range (IQR) are listed for continuous variables. Stages were coded as: ADC stage-0, not impaired; stage-0.5, having subclinical impairment; stage-1, mildly impaired; stage-2, moderately impaired. Plasma HIV RNA was defined as undetectable when the viral load is <=400 copies/mL. CSF HIV RNA was defined as undetectable when the viral load is <=75 copies/mL.

Continuous variables	Total N	Median	IQR
Nadir CD4+ (cells/mm^3)	210	37	[13–91.75]
CD4+ (cells/mm^3)	204	328	[214–474]
Duration of HIV (years)	210	12	[8–18]
CPE score	198	1.5	[1–2]
Years on cART	177	1.6	[0.7–3.3]

Categorical variables	Total N	Categories	n (%)	Binary
ADC stage	200	Stage-0	122 (61%)	0
		Stage-0.5	51 (25%)	0
		Stage-1	24 (12%)	1
		Stage-2	3 (2%)	1
Plasma HIV RNA	202	Undetectable	170 (84%)	1
		Detectable	32 (16%)	0
CSF HIV RNA	60	Undetectable	43 (72%)	1
		Detectable	17 (28%)	0

2.4. Proton magnetic resonance spectroscopy (^{1}H-MRS)

The ^{1}H-MRS protocol has been previously described (Cohen et al., 2010a; Harezlak et al., 2011). Briefly, levels of cerebral metabolites *N*-acetylaspartate (NAA), *myo*-inositol (MI), choline-containing compounds (Cho), glutamate/glutamine (Glx), and creatine (Cr) were measured by single-voxel ^{1}H spectra using a PRESS pulse sequence. Voxels 6 ml were prescribed in three regions: gray matter in mid-frontal cortex (MFC), right or left mid-frontal white matter in *centrum semiovale* (FWM), and right or left deep gray matter in basal ganglia (BG). Field homogeneity and water suppression were adjusted using automated algorithms provided by the manufacturer. Water-suppressed spectra were collected with echo time/repetition time (TE/TR) of 35/3000 ms, bandwidth 2500 Hz, 128 averages. MRS data were acquired using matched pulse sequence parameters on GE and Siemens MRI units. In addition to the water-suppressed MRS acquisition, single-scan fully relaxed unsuppressed water FIDs were acquired from each voxel at seven different echo times (TE = 30, 45, 65, 100, 200, 500, and 1500 ms; TR = 15 s). These data were used to infer the voxel's CSF content which was used in the metabolite concentration computations. To control for a possible instrument bias, we collected phantom MRS data concurrently with the subject evaluation, using the same protocol described above.

The time domain spectral data were transferred to a central MRS processing site, at the John A. Burns School of Medicine, University of Hawaii (site PI: Thomas Ernst). MR spectra were evaluated for quality based on visual inspection and the %SD (Cramer–Rao lower bounds) and FWHM outputs from the LC Model spectral analysis software (Provencher, 2001). Concentrations of metabolites NAA, MI, Cho, Glx and Cr were computed using LC Model with unsuppressed water FID at TE = 35 ms used for eddy-current correction. The MRS signals produced by glutamine and glutamate overlap almost completely in 1.5 T human brain spectra. This introduces a confound into the LC Model signal quantification algorithm, which leads to incorrect assignment of glutamate signal to glutamine and vice versa. Accordingly, as has been customary for LCModel processing of 1.5 T brain spectra for many years, we report only the sum of the glutamate and glutamine concentrations (Glx) in this work. Both absolute concentration and metabolite/Cr ratio were computed for each metabolite and used in our analyses. This automated processing method yields metabolite concentration estimates with coefficient of variation <15% (Lee et al., 2003). The variability in measurements of metabolite ratios over the group of human subjects was about 3-fold larger than the variability measured in the phantoms. The variability in the phantom metabolite ratio

measurements between the seven sites did not exceed 7% of the overall mean, with most of the variation falling within 2–3%. Because the phantom agreement between sites (including between acquisitions) that used Siemens and GE scanners was within a few percent, we did not make scanner-specific corrections to the derived metabolite concentrations and ratios.

2.5. Missing values

The Data Coordinating Center at the Indiana University School of Medicine followed strict data collection procedures that were put in place in the HIVNC study protocol. Most data were available for all 210 patients reported in this manuscript. However, missing entries are unavoidable in a large multi-site study. MRS data for most regions and metabolites had between 3.8% and 7.1% values missing. The only exceptions are metabolites in the basal ganglia, where 11.4% to 13.8% values were missing, and Glx values in all brain regions where about 90% of the region-specific values are collected. The reasons for missing data are two-fold: first, the subcortical location of the basal ganglia voxel is especially susceptible to CSF interference resulting in poor metabolite estimates; second, Glx concentrations are harder to estimate than the other four metabolites. The metabolite concentrations were quantified using the package LC Model (Provencher, 1993). The fitting results are given both as absolute concentrations and as ratios to the total Cr Level. The estimated concentrations were used in further analysis only when the metabolite concentration was estimated with the Cramer–Rao lower bound (CRLB) $\leq$20%. In other words, the MRS data were acquired for all subjects, except for a small number which were excluded for quality and technical reasons. Using a 1.5 T magnetic field strength, four metabolites (NAA, Cr, Cho, mI) can be estimated well for most spectra. However, Glx estimation is harder, and frequently the estimates were rejected by the CRLB criterion.

2.6. Tensor-based morphometry (TBM)

For TBM analysis of the anatomical images, pre-processing steps included N3 bias field correction (Sled et al., 1998), and automated linear registration to a target brain template using 12-parameter affine registration (Collins et al., 1994). Globally aligned images were resampled with an isotropic matrix of 220 voxels in the *x*-, *y*-, and *z*-dimensions; each interpolated voxel was 1 mm × 1 mm × 1 mm in size.

Using the registered images, an unbiased group average template, called a minimal deformation target (MDT), was created to serve as the target for nonlinear registration. MDT construction is detailed in prior papers (Hua et al., 2008, 2009).

To quantify 3D patterns of volumetric tissue change, all globally aligned individual brain images were non-linearly registered to the MDT, using inverse-consistent elastic intensity-based registration (Leow et al., 2005). A Jacobian matrix field was derived from the gradients of the deformation field that aligned an individual brain to the MDT template. The determinant of the local Jacobian matrix was derived from the forward deformation field to characterize local volume differences. Color-coded Jacobian determinants were used to illustrate regions of volume expansion, i.e. those with det $J(r) > 1$, or contraction, i.e. det $J(r) < 1$, relative to the group template (Ashburner and Friston, 2003; Chung et al., 2001; Freeborough and Fox, 1998; Riddle et al., 2004; Thompson et al., 2000; Toga, 1999). As all images were registered to the same template, these Jacobian maps share a common anatomical coordinate defined by the MDT. Individual Jacobian maps were retained for further statistical analyses.

Given the cross-sectional nature of this study and the fact that it included only HIV positive individuals, the references to "atrophy" are indirect. Brain atrophy in this manuscript refers to less brain tissue or greater CSF expansion relative to the average brain template.

2.7. Voxel-wise linear regressions

At each voxel in the brain, multiple linear regression was used to model relationships between structural brain differences (Jacobian determinant values) and cerebral metabolite levels as well as nadir CD4+ count, after controlling for age, sex, and ethnicity. Ethnicity (E) was coded using 2 dummy variables, African Americans were coded as "1" for E1 only, and "Others" (including Asians, Native Americans and American Indians) were coded as "1" for E2 only, while Caucasians were coded as "0" for both E1 and E2. Cerebral metabolite variables included absolute levels of NAA, MI, Cho, Glx, and Cr, and metabolite ratios of NAA/Cr, Cho/Cr, MI/Cr, and Glx/Cr, in MFC, FWM, and BG areas. We modeled region brain volumes by fitting the following multiple regression model at each voxel:

$$Jacobian = \beta_0 + \beta_1 \cdot Age + \beta_2 \cdot Sex + \beta_3 \cdot E1 + \beta_4 \cdot E2 + \beta \cdot Covariate\_of\_interest + error$$

We used this voxel-wise multiple regression to assess whether the local brain volume differences (regional brain volume differences relative to the MDT) were significantly associated with the covariates of interest. Statistical or "*p*-value" maps were generated to visualize patterns of voxel-wise significance. The significance maps (uncorrected) were subsequently corrected for multiple comparisons using the standard false discovery rate (FDR) method, with the conventionally accepted false-positive rate of 5% ($q = 0.05$) (Benjamini and Hochberg, 1995). The FDR correction was applied to two-sided tests, inside the whole brain, without considering the sign of partial regression coefficients (β-values). The uncorrected maps were thresholded with the FDR critical *P*-values; the surviving voxels (or suprathreshold voxels) are expected to have no more than 5% false positives. In other words, it is expected that the voxel-by-voxel associations are true associations at 95% of the suprathreshold voxels shown. The color-coded maps of β-values, displayed over the MDT, represent areas of significant association, where the estimated degree of tissue deficit or excess is displayed at each voxel (as a percentage, relative to the template) that is associated with brain metabolite or clinical measures, after controlling for age, sex, ethnicity, and multiple comparisons.

2.8. Evaluating the relative importance of predictors and ranking the overall effect sizes

To assess the relative importance of predictors in a linear regression model, we calculated *T*-statistics on the partial regression coefficients (β-values) at voxels that passed FDR correction. We provided summaries of mean and standard deviations for both the β-values and the *T*-statistics, separated into two groups showing positive and negative associations. Due to the high spatial resolution of the voxel-wise association study, none of the summaries above provides a definitive measure of importance of the predictors in a multiple linear regression model. They offer information about the spatial variability and relative strength of the statistical associations.

The volume of significant voxels that passed the FDR critical *P*-value (corrected for multiple comparisons) was used to define the overall effect sizes as "areas of significance". The effect size was measured both in terms of the number of voxels and as a percentage of the overall brain volume, which are interchangeable. We note that there is no standard way to rank the effect size in a statistical map, as it depends on whether a large difference in a few voxels is considered greater than a widespread diffuse effect.

3. Results

3.1. Brain atrophy is correlated with cerebral metabolite levels

We set out to find which of the available MRS measures best predicted brain atrophy. After controlling for age, sex, and ethnicity, and

correcting for multiple comparisons, regional brain volumes were significantly associated with absolute levels of (1) NAA measured in all three brain regions of interest (FWM, BG, and MFC), (2) Glx in BG and MFC, (3) Cr in MFC, (4) Cho in MFC, and (5) MI in MFC (Tables 3 and 4). Disrupted cerebral metabolite levels were linked to greater brain atrophy, as reflected by less brain tissue or greater CSF expansion relative to the average brain template. Although two-tailed statistical tests were used, we separated the results into positive (Table 3) and negative (Table 4) associations to make clear the directions of association. The effect size was summarized as the number of significant voxels passing the FDR critical *P*-value, and equivalently, as a percentage of the whole brain. We also examined the mean and standard deviation of the partial regression coefficient (β-value), *T*-statistics, and areas of significance.

In a separate analysis, the relative metabolite concentrations were calculated with reference to the levels of Cr (Tables 3 and 4). Glx/Cr and NAA/Cr, measured in the basal ganglia, remained strong predictors of brain atrophy. Compared to the absolute measures, all relative metabolite concentrations (NAA, Glx, Cho, and MI) measured in the MFC area and NAA measured in the FWM were no longer associated with brain volume variations. Additionally, MI/Cr, Cho/Cr, and Glx/Cr measured in the FWM showed significant correlations with regional brain volumes, while their absolute counterparts did not show a significant association.

When ranking the absolute and relative metabolite analyses together, the top two metabolites were absolute concentrations of Glx in BG (positive associations: 375,095 significant voxels/20% of the total brain volume; negative associations: 223,333 voxels/12%; overall: 598,428 voxels/32%) and NAA in FWM (positive associations: 512,139 significant voxels/27% of total brain volume; negative associations: 40,448 voxels/2%; overall: 552,587 voxels/29%) (Tables 3 and 4). Partial regression coefficient maps show the associations between atrophy profiles and metabolite levels for Glx in the BG (Fig. 1) and NAA in the FWM (Fig. 2). Higher levels of Glx in the BG and lower levels of NAA in FWM were associated with lower white matter volume and greater ventricle/CSF expansion; these results are in the hypothesized direction.

Generally, cerebral white matter deficits (lower volumes) were associated with lower absolute NAA concentrations measured in FWM and BG as well as NAA/Cr in BG, (2) higher absolute Glx concentrations in the BG, Glx/Cr in BG, MI/Cr in FWM, Cho/Cr in FWM. Volume deficits in the deep brain nuclei, such as the putamen, were linked to lower levels of NAA, Cr, Glx, Cho, and MI measured in the mid-frontal gray matter, or MFC.

3.2. Brain atrophy linked to nadir CD4 + cell count

Nadir CD4+ cell count represents the history of greatest immunosuppression. After controlling for demographic factors and multiple

Table 2
Summary of absolute and ratio of MRS metabolite levels inside each region-of-interest (ROI) in the participant cohort, showing the number of subjects with available data (N), minimum (Min) and maximum (Max) values, group mean (Average) and standard deviation (SD).

	ROI	N	Min	Max	Average	SD
Absolute						
NAA	FWM	202	5.5	11.5	8.2	1.12
	BG	186	4.0	10.5	7.9	1.19
	MFC	197	2.8	9.0	6.8	1.09
Cr	FWM	202	3.2	7.6	4.9	0.63
	BG	186	2.1	8.0	5.3	0.84
	MFC	197	1.9	7.5	4.7	0.80
Cho	FWM	202	0.8	4.4	1.7	0.38
	BG	186	0.7	4.5	1.5	0.33
	MFC	197	0.4	2.1	1.2	0.28
MI	FWM	202	1.3	11.3	5.1	1.13
	BG	182	1.2	6.7	4.2	0.86
	MFC	196	1.9	8.0	4.4	1.03
Glx	FWM	185	3.2	14.7	8.2	1.71
	BG	164	4.4	14.8	10.2	2.20
	MFC	181	3.5	14.0	9.8	1.72
Ratio						
NAA/Cr	FWM	202	1.2	2.3	1.7	0.20
	BG	184	1.0	2.1	1.5	0.24
	MFC	196	1.0	1.9	1.5	0.14
Cho/Cr	FWM	202	0.2	0.5	0.3	0.06
	BG	184	0.2	0.4	0.3	0.05
	MFC	196	0.1	0.4	0.3	0.04
MI/Cr	FWM	201	0.5	1.8	1.1	0.21
	BG	181	0.3	1.3	0.8	0.18
	MFC	195	0.4	1.5	0.9	0.14
Glx/Cr	FWM	184	0.7	2.6	1.7	0.32
	BG	164	0.8	3.1	1.9	0.38
	MFC	181	1.3	3.0	2.1	0.29

Table 3
Positive associations (i.e., with positive β-values) are shown here between metabolite levels and brain volumes, listing the effect size as the number of significant voxels passing the FDR critical *P*-value (and as a percentage of the entire brain). We also report the mean (standard deviation-SD) of the β-values within the areas declared significant, mean (SD) of the *T*-statistics, and areas of significance.

Metabolite	Effect size	β-values mean (SD)	*T*-statistics mean (SD)	Areas
Absolute				
NAA in FWM	512,139 (27%)	2.2 (0.6)	3.2 (0.5)	Whole brain WM
NAA in BG	264,643 (14%)	2.2 (0.5)	3.3 (0.5)	Whole brain WM
NAA in MFC	94,268 (5%)	2.1 (0.5)	4.0 (1.0)	Thalamus, putamen, midbrain, medial orbital gyrus
Glx in BG	375,095 (20%)	1.3 (0.4)	3.3 (0.7)	CSF/ventricles
Glx in MFC	34,077 (2%)	1.2 (0.2)	3.8 (0.5)	Putamen, midbrain
Cr in MFC	49,123 (3%)	2.5 (0.5)	4.1 (0.7)	Thalamus, putamen, midbrain
Cho in MFC	9478 (1%)	6.7 (0.8)	4.2 (0.5)	Putamen, midbrain
MI in MFC	1847 (0.1%)	2.0 (0.3)	4.4 (0.2)	Putamen
Ratio				
NAA/Cr in BG	43,102 (2%)	11.3 (2.2)	3.4 (0.3)	Frontal and parietal WM
Glx/Cr in BG	267,511 (14%)	6.4 (1.7)	3.2 (0.6)	CSF
Glx/Cr in FWM	15 (0.001%)	7.8 (0.4)	3.9 (0.02)	CSF
Cho/Cr in FWM	85,985 (5%)	41.3 (7.8)	3.5 (0.4)	CSF
MI/Cr in FWM	92,851 (5%)	15.5 (8.2)	3.2 (0.5)	CSF/ventricles

Table 4
Negative associations (negative β-values) between metabolite levels and brain volumes, listing the effect size as the number of significant voxels passing the FDR critical P (and as a percentage of the entire brain). We also report the mean (standard deviation-SD) of the β-values within the areas declared significant, mean (SD) of the *T*-statistics, and areas of significance.

Metabolite	Effect size	β-values mean (SD)	*T*-statistics mean (SD)	Areas
Absolute				
NAA in FWM	40,448 (2%)	−3.6 (1.5)	−3.0/0.4	CSF/ventricles
NAA in BG	56,573 (3%)	−3.5 (1.6)	−3.3/0.4	CSF/ventricles
NAA in MFC	59,819 (3%)	−4.4 (1.8)	−3.7/0.5	CSF/ventricles, cerebellum
Glx in BG	223,333 (12%)	−1.3 (0.3)	−3.3/0.7	Whole brain WM
Glx in MFC	31,009 (2%)	−2.4 (0.9)	−3.5/0.3	CSF/ventricle, cerebellum
Cr in MFC	31,973 (2%)	−6.0 (2.2)	−3.6/0.4	CSF/ventricles
Cho in MFC	0	0		None
MI in MFC	0	0		None
Ratio				
NAA/Cr in BG	52,639 (3%)	−17.3 (7.5)	−3.4/0.2	CSF
Glx/Cr in BG	255,298 (14%)	−7.5 (2.0)	−3.4/0.6	Whole brain WM
Glx/Cr in FWM	5622 (0.3%)	−12.5 (2.1)	−4.2/0.2	Cerebellum (inferior tonsil area)
Cho/Cr in FWM	6605 (0.4%)	−35.7 (7.3)	−3.3/0.2	Parietal WM
MI/Cr in FWM	267,932 (14%)	−12.5 (3.2)	−3.3/0.5	Whole brain WM

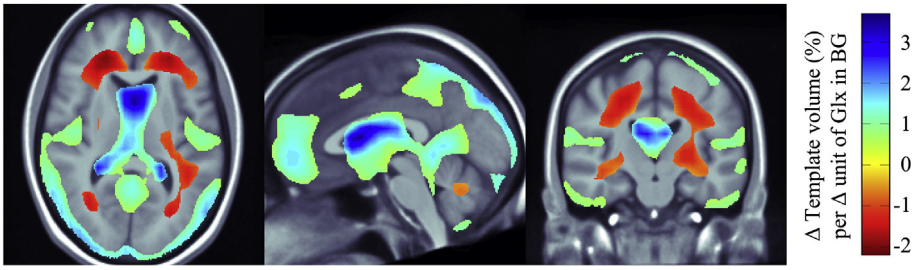

Fig. 1. *Brain atrophy relates to Glx levels measured in BG.* 3D maps show regions where the absolute Glx concentrations measured in basal ganglia are significantly associated with regional brain volumes, after controlling for age, sex, ethnicity, and multiple comparisons. Displayed over the MDT, the color-coded regression coefficients, β-values, are shown at each voxel, representing the estimated degree of tissue deficit or excess at each voxel (as a percentage, relative to the template) that is associated with the Glx concentrations measured in BG. Multiple comparisons across voxels are corrected with a regional FDR method; only voxels that survive this statistical correction are shown in color. (For interpretation of the references to color in this figure legend, the reader is referred to the web version of this article.)

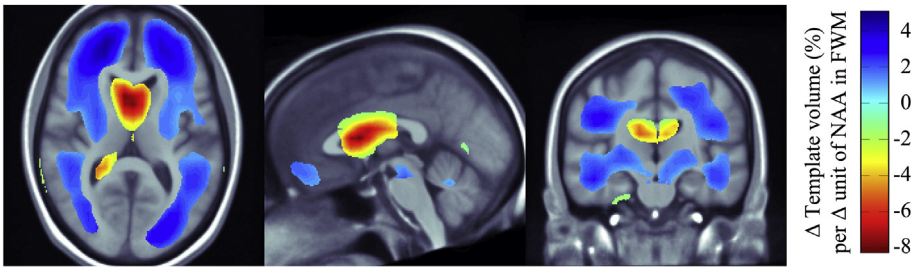

Fig. 2. *Brain atrophy relates to NAA levels measured in FWM.* Here we show brain regions where the absolute NAA concentrations measured in frontal white matter are significantly associated with regional brain volumes, after controlling for age, sex, ethnicity, and multiple comparisons. Displayed over the MDT, the color-coded regression coefficients, β-values, are shown at each voxel, representing the estimated degree of tissue deficit or excess at each voxel (as a percentage, relative to the template) that is associated with NAA concentrations (in absolute units). Multiple comparisons across voxels are corrected with a regional FDR method; only voxels that survive this statistical correction are shown in color. (For interpretation of the references to color in this figure legend, the reader is referred to the web version of this article.)

comparisons, poorer immunosuppression history predicted the degree of brain atrophy (Fig. 3). Lower nadir CD4+ count was associated with greater atrophy (positive β-values in Fig. 3), in a broad region encompassing frontal and parietal white matter bilaterally, and the cerebellum. For every 25-point reduction in nadir CD4+ cell count, there was a 1–2% greater volume deficit, on average, in regional white matter volumes (regression coefficients β ranged from 0.04 to 0.08%). CSF volume showed a negative correlation with nadir CD4+ counts — as expected, since CSF spaces expand when adjacent tissue is atrophied. The other clinical measures, including current CD4+ count, ADC stage, HIV RNA concentration in plasma or CSF, duration of HIV infection, CPE scores, and years on cART, were not significantly related to brain volume after controlling for demographic factors, and correcting for multiple comparisons.

3.3. Ranking of overall effect sizes

As predictors of atrophy, we ranked absolute and relative metabolites as well as nadir CD4+, to compare the strengths of their statistical associations with brain atrophy (Fig. 4). As defined in the methods, a larger effect size generally denotes a more widespread effect on the brain, while a smaller effect size is typically regional, or detected in a more restricted pattern. Nadir CD4+ demonstrated the highest effect size as a predictor of brain atrophy, with 35% of the total brain volume showing significant correlations with nadir CD + counts. Absolute measures of metabolites generally showed higher effect sizes compared to their ratios (metabolite/Cr). Among the absolute metabolite measures, Glx in BG and NAA in FWM demonstrated the strongest associations with volume deficits throughout the brain. The top two associations

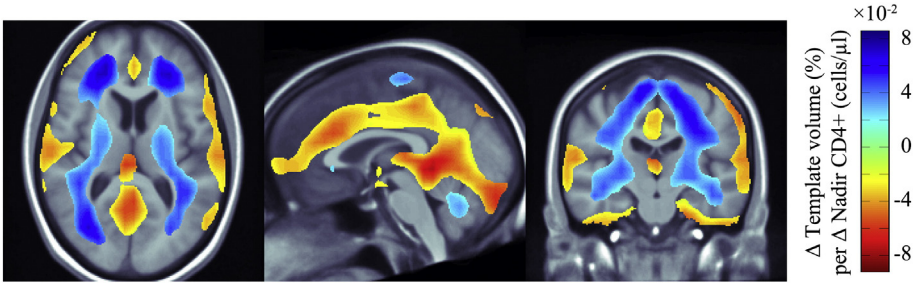

Fig. 3. *Brain atrophy relates to nadir CD4 + counts.* In people with lower nadir CD4+ counts, brain atrophy is greater in a broad region that encompasses much of the deep white matter (*blue colors denote a positive correlation, with lower volumes in people with low CD4 + counts*). In brain regions where nadir CD4+ counts are significantly associated with white matter volume, the regression coefficients, β, are shown at each voxel. Results shown are corrected for multiple comparisons, by thresholding them at the critical p-value. The β-values represent the estimated degree of tissue deficit – or enlargement, for CSF spaces – at each voxel (in percentage relative to the template) that is associated with the nadir CD4+ count, after controlling for age, sex, and ethnicity. For each 25-point reduction in nadir CD4+, there was, on average, a 1–2% greater deficit in white matter volume (in blue regions: β-values range from 0.04 to 0.08%, so 25 times this amounts to a 1–2% volume deficit relative to the template). (For interpretation of the references to color in this figure legend, the reader is referred to the web version of this article.)

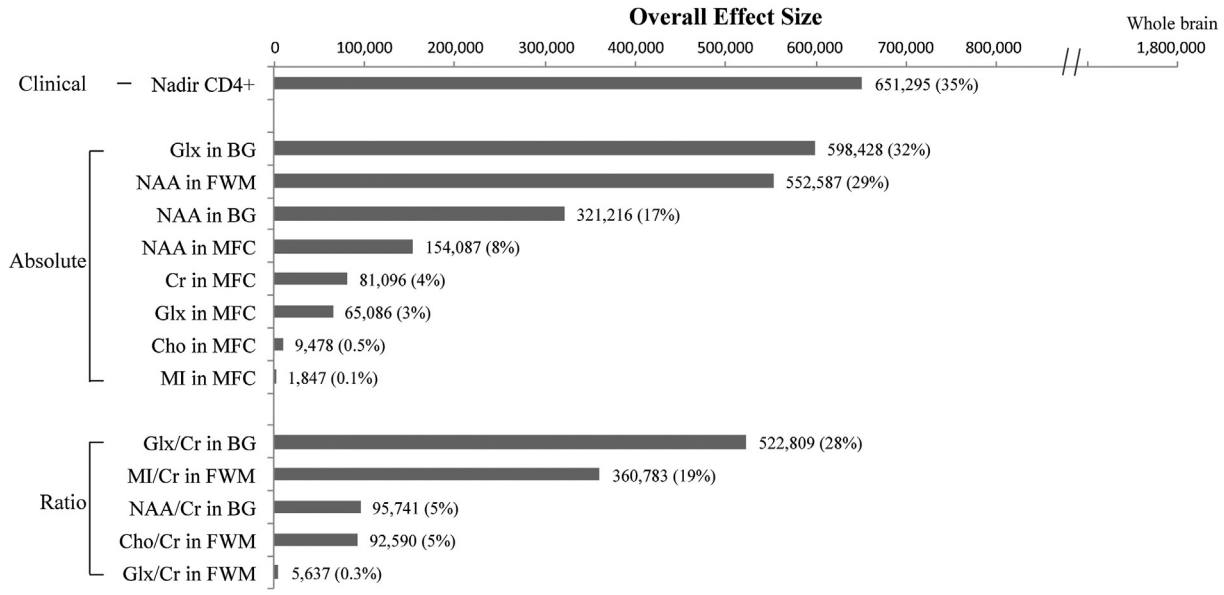

Fig. 4. *Which measures best predict brain atrophy?* Here we show an ordered ranking of predictors of brain atrophy, divided into clinical characteristics (*top*), absolute values (*middle*) and ratios (*bottom*) of brain metabolite levels. The ranking here is based on the overall effect size, as indicated by the number of significant voxels passing the FDR correction (percentage of the whole brain). This method considers the ability of each measure to predict brain atrophy diffusely throughout the brain, considering both the size of the effect on brain volume, and the proportion of the brain showing detectable associations.

for the metabolite ratios were found for Glx/Cr in the BG and MI/Cr in the FWM.

4. Discussion

This study is the first analysis to use TBM to map and understand the 3D profile of regional brain volume variations in a group of 210 HIV-infected individuals on stable cART. We identified a broad range of brain regions where the degree of volumetric atrophy was related to metabolite levels in various key brain substructures, including the basal ganglia, frontal white matter, and medial frontal cortex. Unlike the traditional ROI-based approach, TBM can detect and map the profile of diffuse white matter effects, adding a new dimension by mapping voxel-wise white matter and subcortical volume deficits along with their associations in the context of chronic disease and cART. Our two main findings were that (1) lower nadir CD4+ count was strongly associated with cerebral white matter deficits; and (2) disruptions or alterations in region specific metabolites were linked to local and widespread deficits in brain volume. These results are largely in line with expectations, with the added benefit of mapping the profile of effects in 3D throughout the brain.

Nadir CD4+ count reflects the history of greatest immunosuppression and is a major risk factor for neurocognitive impairment in people undergoing treatment for HIV infection. While prior studies have consistently demonstrated the relationship between lower nadir CD4+ count and greater brain deficits in white matter and subcortical gray matter volumes, the correlates in the brain of other HIV clinical measures are somewhat inconsistent (Cohen et al., 2010b; Jernigan et al., 2011; Tate et al., 2011). In our study, which is relatively well powered given the large sample, we did not find significant associations between brain volume and other clinical measures. Prior reports have shown that detectable plasma HIV RNA, current CD4+ count, duration on cART, and ADC stage were associated with brain volume deficits (Cohen et al., 2010b; Jernigan et al., 2011; Tate et al., 2011). Findings in MRS metabolites were largely consistent with existing literature except for Glx (Cohen et al., 2010a; Mohamed et al., 2010). These discrepancies may be due to differences in sample size and patient inclusion criteria. Some of the differences in the clinical correlations may be due to the image analysis approaches (ROI based methods vs. unbiased TBM), which will be discussed later.

In prior studies from the same consortium, absolute and relative metabolite concentrations were associated with gray matter and ventricular volumes, but not with the total white matter volume (Cohen et al., 2010a). Lower nadir CD4+ count was associated with a lower *total* white matter volume, but without anatomical details on the affected regions (Cohen et al., 2010b) and with decreases in corpus callosum areas in another HIVNC study (Tate et al., 2011). The current study identified several white matter regions where atrophy was associated with brain metabolite levels, and with nadir CD4+ count. Glx levels measured in BG were primarily linked to frontal white matter deficits and CSF expansion (Fig. 1), while the effects of NAA measured in FWM and nadir CD4+ count were more widespread, affecting the whole brain white matter while showing greater associations in the frontal lobes (Figs. 2 and 3). Additionally, a broad spectrum of metabolite disturbance, including NAA in MFC, Glx in BG, Glx in MFC, Cho in MFC and MI in MFC, was shown to correlate with volume deficits in subcortical structures such as thalamus, putamen, and midbrain (Table 3). These findings were consistent with the hypothesized primary involvement of the frontal–striatal networks in HIV (Dal Pan et al., 1992; Navia et al., 1986a, 1986b; Tate et al., 2009). Our study differs in two respects compared to the prior studies in the same cohort. First, we used a larger sample ($N = 210$, compared to $N = 67$ in Cohen et al., 2010a and N = 82 in Cohen et al., 2010b). Assuming other factors are comparable, this provided greater statistical power to detect subtle effects. Second, we used a voxel-wise analysis technique that does not rely on accurate regional segmentation of the white matter, allowing the detection of diffuse white matter effects while pinpointing regions of significance, which was previously unobtainable with a traditional ROI-based approach.

4.1. HIV clinical characteristics and brain atrophy

4.1.1. Immunosuppression

HIV selectively infects and destroys monocytes and T helper cells (a type of lymphocyte) that express the surface protein CD4+. The levels of CD4+ T cells in blood are important indicators of immunosuppression. Some prior studies report that decline of current CD4+ T cell counts was correlated with cognitive decline, cortical gray matter

thinning in the frontal and language areas (Thompson et al., 2005), corpus callosum volume reduction (Thompson et al., 2006), and ventricular expansion (Thompson et al., 2006). Higher current CD4+ count, indicating better immune system status, was unexpectedly correlated with lower white matter and subcortical gray matter volumes as well as increased CSF (Jernigan et al., 2011). The difference in the effect of current CD4+ count is likely due to disparities in treatment effect, duration of treatment, or neuroinflammatory mechanism in response to a combination of viral infection and treatment (Jernigan et al., 2011). In our study, we did not detect a significant effect of current CD4+ count on brain atrophy. Nadir CD4+ counts, the lowest CD4+ count measured after HIV infection, predict poor immune recovery (Negredo et al., 2010), neurocognitive impairment (Ellis et al., 2011), and white matter volume deficits (Cohen et al., 2010b; Jernigan et al., 2011; Tate et al., 2011) in patients receiving cART. Here we found that lower nadir CD4+ T cell counts (cell counts before cART initiation), but not current CD4+ T cell counts, were strongly linked to regional white matter deficits across the brain. We showed for the first time a quantitative relationship between a reduction in nadir CD4+ and its effect on volume loss in the white matter (1–2% decrease for every 25 point reduction in nadir CD4+). To further understand the contribution of nadir CD4+ count to brain volume, we compared its effect with the cerebral metabolites also associated with brain loss and found that the nadir CD4+ showed the strongest effect size. Together these findings support the predictive value of nadir CD4+ for subsequent brain atrophy, and the potential importance of early initiation of cART in preventing brain damage.

4.1.2. Other HIV clinical characteristics

We did not find a significant correlation between regional brain volumes and the other clinical measures, including current CD4+ count, ADC stage, HIV RNA concentration in plasma or CSF, duration of HIV infection, CPE scores, and years on HAART, after controlling for demographic factors and correcting for multiple comparisons. Prior studies have shown lower corpus callosum areas in HIV-positive subjects compared with healthy controls, but a lesser difference was found when comparing the symptomatic group (ADC stage ≥ 1) versus those who were asymptomatic (ADC stage 0) or had subclinical impairments (ADC stage 0.5); no significant differences were found in any of the corpus callosum areas between asymptomatic subjects (ADC stage 0) and subjects with subclinical impairment (ADC stage 0.5) (Tate et al., 2011). This suggests that the hypothesized linear relationship between cognitive impairment and structural brain loss might be quite weak, as cognitive decline typically lags behind structural brain impairment. Additionally, the current study had a smaller percentage of patients with advanced ADC stage (ADC stage ≥ 1, 14% of the cohort), in part due to the lower incidence of cognitive impairment since the advent of cART (Ances and Ellis, 2007; McArthur et al., 2004). Even so, the unbalanced sample might have limited the statistical power to detect the effect. Other reports have shown that detectable plasma HIV RNA was related to less total white matter (Jernigan et al., 2011) and abnormalities in basal ganglia (Cohen et al., 2010b). Additionally, longer exposure to cART was associated with lower white matter volume (Jernigan et al., 2011).

The inclusion criteria in the current study included nadir CD4+ cell count less than 200 cells/mm^3 (mean = 61, standard deviation = 58), while the upper range of nadir CD4+ in Jernigan et al. (2011) was 1104 cells/mm^3 (mean = 190, standard deviation = 183). The differences in inclusion criteria suggest that patients in the current study might have a history of greater immunosuppression compared to the ones in the Jernigan study. This may account for some of the differences in findings.

4.2. Cerebral metabolite disruptions in chronic HIV infection

Cerebral metabolite disruptions are another consequence of HIV infection, and they typically indicate neural injury and inflammatory responses in the brain. ^{1}H-MRS provides a sensitive and noninvasive *in vivo* method to detect these changes. Before the routine use of cART, HIV+ patients were consistently reported as showing (1) reduced NAA (or NAA/Cr) — a marker of neuronal metabolism, (2) elevated Cho (Cho/Cr) — a marker of cell membrane damage, or (3) elevation in MI (MI/Cr) — a glial cell marker (Chang et al., 1999; Lopez-Villegas et al., 1997; Meyerhoff et al., 1999; Paley et al., 1996; Salvan et al., 1997; Tracey et al., 1996). *In vivo* MRS studies have consistently demonstrated cerebral metabolite disturbance in HIV infected brains, confined to the deep gray and white matter, and correlated with the severity of neurocognitive impairment (Budka et al., 1991; Glass et al., 1993; Navia and Rostasy, 2005; Navia et al., 1986b; Rostasy et al., 1999; Tracey et al., 1996). In patients with chronic HIV infection on stable treatment, neural injury and inflammation measured by MRS as well as cognitive impairment persist in the setting of cART (Cysique et al., 2004; Harezlak et al., 2011). Analyzing a similar but smaller cohort (N = 67), cerebral metabolite abnormalities were correlated with total gray matter but not white matter volume (Cohen et al., 2010a). Those analyses are further enriched in this study, where we examined brain atrophy in greater detail, using TBM to map 3D patterns of regional (voxel-wise) brain deficits in 210 patients with HIV. We further showed that when ranking the metabolite effects alone, decreases in NAA in frontal white matter and increases in Glx in the basal ganglia had the strongest associations with loss of brain volume, supporting the pathogenic importance of these metabolites in the regional and global structural integrity of the HIV brain.

Findings in Glx are slightly discordant with a previous MRS study in HIV-infected individuals by Mohamed et al. (2010), which showed *lower* levels of Glx and a lower Glx/Cr ratio in FWM in patients with HIV-associated dementia. Our study showed an association between Glx elevation in the BG and brain volume deficits, with smaller effects observed with Glx measured in FWM. However, this may be due to several differences between the two studies including the scanner field strength (1.5 T vs. 3.0 T), inclusion criteria (no nadir CD4+ count cutoff in Mohamed et al.), sample size (210 in this study vs. 86 patients in Mohamed et al.) and the analysis (here, correlations with morphometry and, in the other paper, Glx differences among groups). A common inference from our study and that of Mohamed et al. is that the glutamate (Glu)-glutamine (Gln) cycle is dysregulated in HIV+ cohorts. The "Glx" signal is defined as the sum of the local concentrations of glutamate (Glu) and glutamine (Gln), so an increase in Glx may be due to one or both of these components. The synthesis of Glu in neurons depends on glial re-uptake, and its conversion to Gln, which then enters neurons and is converted to Glu, in order to resume the cycle (Gruetter et al., 2003). One interpretation of our data is that elevated levels of Glu may lead to neuronal excitotoxicity followed by neuronal death and decreases in NAA – a neuronal and mitochondrial marker – and tissue loss. In support of this, a recent study has shown in a human microglia primary culture system that infected microglia are associated with a significant increase in extracellular Glu. Elevated levels of the glutamate-generating enzyme glutaminase isoform C are also found in *post-mortem* brain tissue of HIV patients with dementia compared to HIV-negative controls (Huang et al., 2011).

4.3. Absolute versus relative MRS metabolite levels

We examined associations of brain volumes with two different brain metabolites, including their absolute concentrations and ratio to levels of Cr. Our prior analysis suggested that the absolute metabolite concentration is a more robust predictor of brain changes and cognitive function, compared to the ratio (Cohen et al., 2010a). Because absolute measures lack a reference, we used MRS phantom data as a correction, offering a reference value. We acknowledge that the phantom correction only partially addresses the issue. Relative metabolite concentrations were calculated by dividing the absolute measures by the mean Cr level inside the same region; however, as shown here, Cr level also varies by clinical status, and therefore it is not really an inert reference

value unaffected by the metabolic state of the individual. In our analysis, the absolute concentration of Cr in the MFC independently correlated with subcortical volumes (Tables 3 and 4). We observed a contrasting effect of Cr in MFC and FWM especially. By using Cr as the denominator in our analyses, the correlations between brain volumes and metabolite levels (NAA, Glx, MI, Cho) in MFC were weakened or eradicated, while the correlations with Glx, MI, and Cr in FWM were established or further strengthened.

4.4. Clinical implications

The results in this manuscript provide further evidence of widespread disturbances in neurological function in the setting of stable disease, and offer new insights into possible dynamic relationships between metabolic and structural injury in the HIV infected brain. This underscores the importance of monitoring neurological function in chronically infected patients, particularly those with a history of advanced immunosuppression who appear to be at greatest risk of developing cerebral atrophy even in the setting of cART therapies. The effect size analysis of the MRS metabolites pinpoints for the first time the relative importance of NAA and Glx to predict brain atrophy, suggesting that MRS derived metabolites may provide useful predictors. The combination of MRS and TBM analyses provides a useful approach to interrogate the extent of metabolic and structural injury and could serve as endpoints in clinical trials with neural restorative or protective agents. The effect size analysis of all variables showed that the nadir CD4+ count is the most effective predictor of brain atrophy. This extends recent observations and further supports the hypothesis that early antiretroviral intervention may offer an effective approach to prevent or lessen brain atrophy over time, although future prospective studies are needed to confirm this.

4.5. Areas of significance as a measure of effect size

In this study, 'areas of significance' denotes a quantitative measure of effect size by counting the number of voxels that passed FDR correction, as well as a percentage of the suprathreshold voxels relative to overall brain volume. The analyses in this manuscript are based on an unbiased search of the brain, and so the result was not based on prior knowledge of regions of interest or atlas information. This kind of statistical inference is currently accepted as somewhat standard in brain mapping. The signals quantified are first mapped across the brain and then inferences are made on the proportion of the brain where statistics exceed values that would be expected by chance under the null hypothesis.

4.6. Limitations

Although all 210 participants had MRI scan data and nadir CD+ count, there were varying degrees of missing data in clinical characteristics (Table 1) and brain MRS measures of metabolite levels (Table 2). Therefore, the sample sizes varied for some of the statistical tests depending on available data. While the sample sizes did not vary a great deal, the CSF HIV RNA sample was notably small ($N = 60$), so statistical power was lower. Another limitation is that, although nadir CD4+ demonstrated strong associations with brain volume, we did not adjust for nadir CD4+ while performing statistical analysis using other variables. This was difficult from a practical standpoint as we did exploratory analyses with a large number of clinical and MRS measures. With fewer covariates of interest, it would be feasible to modify the model in accordance with a prior hypothesis and explore hierarchical relationship. A new statistical model with all covariates (clinical, MRS and demographic factors) included will strengthen future studies. The statistical significance and effect sizes will be evaluated by finding connected regions showing consistent associations with a set of covariates of interest.

5. Conclusion

Structural and metabolite changes along with neurocognitive impairment persist in the setting of chronic HIV infection and cART treatment for reasons that are not entirely clear. In this study we showed that TBM combined with linear regression modeling offers a sensitive and powerful in vivo measure to map brain deficits in HIV infection and to identify factors linked to alterations in brain structure. Disruptions in specific brain metabolites in the basal ganglia and frontal white matter were associated with volumetric deficits in the white matter and deep brain nuclei. Cerebral white matter deficits were strongly linked to lower nadir CD4+ count. These studies will advance our understanding of how metabolic and atrophic changes unfold in the setting of chronic infection and help pinpoint the underlying factors contributing to such changes.

Abbreviations

ADC	AIDS dementia complex
cART	combined antiretroviral therapies
CNS	central nervous system
CPE	antiretroviral CNS penetration-effectiveness scores
CSF	cerebrospinal fluid
HIVNC	HIV Neuroimaging Consortium
MRI	magnetic resonance imaging
^{1}H-MRS	proton magnetic resonance spectroscopy
^{1}H-MRS	brain metabolites:
-Cho	choline-containing compounds
-Cr	creatine
-Glx	glutamate and glutamine
-MI	*myo*-inositol
-NAA	*N*-acetylaspartate
^{1}H-MRS	key brain substructures:
-BG	right or left deep gray matter in basal ganglia
-FWM	right or left mid-frontal white matter in *centrum semiovale*
-MFC	gray matter in mid-frontal cortex
TBM	tensor-based morphometry

References

Ances, B.M., Ellis, R.J., 2007. Dementia and neurocognitive disorders due to HIV-1 infection. Seminars in Neurology 27 (1), 86–92.

Antinori, A., et al., 2007. Updated research nosology for HIV-associated neurocognitive disorders. Neurology 69 (18), 1789–1799.

Ashburner, J., Friston, K.J., 2003. Morphometry. Human Brain Function. Academic Press.

Benjamini, Y., Hochberg, Y., 1995. Controlling the false discovery rate: a practical and powerful approach to multiple testing. Journal of the Royal Statistical Society: Series B 57, 289–300.

Brew, B.J., et al., 1995. AIDS dementia complex and HIV-1 brain infection: clinical–virological correlations. Annals of Neurology 38 (4), 563–570.

Budka, H., et al., 1991. HIV-associated disease of the nervous system: review of nomenclature and proposal for neuropathology-based terminology. Brain Pathology 1 (3), 143–152.

Cardenas, V.A., et al., 2009. Evidence for ongoing brain injury in human immunodeficiency virus-positive patients treated with antiretroviral therapy. Journal of Neurovirology 15 (4), 324–333.

Castelo, J.M., et al., 2007. Putamen hypertrophy in nondemented patients with human immunodeficiency virus infection and cognitive compromise. Archives of Neurology 64 (9), 1275–1280.

Chang, L., et al., 1999. Cerebral metabolite abnormalities correlate with clinical severity of HIV-1 cognitive motor complex. Neurology 52 (1), 100–108.

Chang, L., et al., 2004. A multicenter in vivo proton-MRS study of HIV-associated dementia and its relationship to age. NeuroImage 23 (4), 1336–1347.

Chen, Y., et al., 2009. White matter abnormalities revealed by diffusion tensor imaging in non-demented and demented HIV+ patients. NeuroImage 47 (4), 1154–1162.

Chiang, M.C., et al., 2007. 3D pattern of brain atrophy in HIV/AIDS visualized using tensor-based morphometry. NeuroImage 34 (1), 44–60.

Chung, M.K., et al., 2001. A unified statistical approach to deformation-based morphometry. NeuroImage 14 (3), 595–606.

Cohen, R.A., et al., 2010a. Cerebral metabolite abnormalities in human immunodeficiency virus are associated with cortical and subcortical volumes. Journal of Neurovirology 16 (6), 435–444.
Cohen, R.A., et al., 2010b. Effects of nadir CD4 count and duration of human immunodeficiency virus infection on brain volumes in the highly active antiretroviral therapy era. Journal of Neurovirology 16 (1), 25–32.
Collins, D.L., et al., 1994. Automatic 3D intersubject registration of MR volumetric data in standardized Talairach space. Journal of Computer Assisted Tomography 18 (2), 192–205.
Cysique, L.A., Maruff, P., Brew, B.J., 2004. Prevalence and pattern of neuropsychological impairment in human immunodeficiency virus-infected/acquired immunodeficiency syndrome (HIV/AIDS) patients across pre- and post-highly active antiretroviral therapy eras: a combined study of two cohorts. Journal of Neurovirology 10 (6), 350–357.
Dal Pan, G.J., et al., 1992. Patterns of cerebral atrophy in HIV-1-infected individuals: results of a quantitative MRI analysis. Neurology 42 (11), 2125–2130.
Davatzikos, C., 1996. Spatial normalization of 3D brain images using deformable models. Journal of Computer Assisted Tomography 20 (4), 656–665.
Ellis, R.J., et al., 2011. CD4 nadir is a predictor of HIV neurocognitive impairment in the era of combination antiretroviral therapy. AIDS 25 (14), 1747–1751.
Fox, N.C., et al., 2001. Imaging of onset and progression of Alzheimer's disease with voxel-compression mapping of serial magnetic resonance images. Lancet 358 (9277), 201–205.
Freeborough, P.A., Fox, N.C., 1998. Modeling brain deformations in Alzheimer disease by fluid registration of serial 3D MR images. Journal of Computer Assisted Tomography 22 (5), 838–843.
Glass, J.D., et al., 1993. Clinical-neuropathologic correlation in HIV-associated dementia. Neurology 43 (11), 2230–2237.
Gongvatana, A., et al., 2009. White matter tract injury and cognitive impairment in human immunodeficiency virus-infected individuals. Journal of Neurovirology 15 (2), 187–195.
Gruetter, R., et al., 2003. Localized in vivo 13C NMR spectroscopy of the brain. NMR in Biomedicine 16 (6–7), 313–338.
Harezlak, J., et al., 2011. Persistence of HIV-associated cognitive impairment, inflammation, and neuronal injury in era of highly active antiretroviral treatment. AIDS 25 (5), 625–633.
Heaton, R.K., et al., 2010. HIV-associated neurocognitive disorders persist in the era of potent antiretroviral therapy: CHARTER Study. Neurology 75 (23), 2087–2096.
Heaton, R.K., et al., 2011. HIV-associated neurocognitive disorders before and during the era of combination antiretroviral therapy: differences in rates, nature, and predictors. Journal of Neurovirology 17 (1), 3–16.
Hua, X., et al., 2008. 3D characterization of brain atrophy in Alzheimer's disease and mild cognitive impairment using tensor-based morphometry. NeuroImage 41 (1), 19–34.
Hua, X., et al., 2009. Detecting brain growth patterns in normal children using tensor-based morphometry. Human Brain Mapping 30 (1), 209–219.
Hua, X., et al., 2013. Unbiased Tensor-based Morphometry: Improved Robustness and Sample Size Estimates for Alzheimer's Disease Clinical Trials. Neuroimage 66, 648–661.
Huang, Y., et al., 2011. Glutaminase dysregulation in HIV-1-infected human microglia mediates neurotoxicity: relevant to HIV-1-associated neurocognitive disorders. The Journal of neuroscience: the official journal of the Society for Neuroscience 31 (42), 15195–15204.
Jahanshad, N., et al., 2012. Disrupted brain networks in the aging HIV+ population. Brain Connectivity 2 (6), 335–344.
Jernigan, T.L., et al., 1993. Magnetic resonance imaging morphometric analysis of cerebral volume loss in human immunodeficiency virus infection. The HNRC Group. Archives of Neurology 50 (3), 250–255.
Jernigan, T.L., et al., 2005. Effects of methamphetamine dependence and HIV infection on cerebral morphology. The American Journal of Psychiatry 162 (8), 1461–1472.
Jernigan, T.L., et al., 2011. Clinical factors related to brain structure in HIV: the CHARTER study. Journal of Neurovirology 17 (3), 248–257.
Lee, P.L., et al., 2003. A multi-center 1H MRS study of the AIDS dementia complex: validation and preliminary analysis. Journal of magnetic resonance imaging: JMRI 17 (6), 625–633.
Leow, A., et al., 2005. Inverse consistent mapping in 3D deformable image registration: its construction and statistical properties. Information Processing in Medical Imaging. Glenwood Springs, Colorado, USA.
Lepore, N., et al., 2008. Generalized tensor-based morphometry of HIV/AIDS using multivariate statistics on deformation tensors. IEEE Transactions on Medical Imaging 27 (1), 129–141.
Letendre, S., et al., 2009. Penetration and effectiveness of antiretroviral therapy in the central nervous system. Anti-Inflammatory & Anti-Allergy Agents in Medicinal Chemistry 8 (2), 169–183.
Lopez-Villegas, D., Lenkinski, R.E., Frank, I., 1997. Biochemical changes in the frontal lobe of HIV-infected individuals detected by magnetic resonance spectroscopy. Proceedings of the National Academy of Sciences of the United States of America 94 (18), 9854–9859.
McArthur, J.C., et al., 2004. Attenuated central nervous system infection in advanced HIV/AIDS with combination antiretroviral therapy. Archives of Neurology 61 (11), 1687–1696.
Meyerhoff, D.J., et al., 1999. Elevated subcortical choline metabolites in cognitively and clinically asymptomatic HIV+ patients. Neurology 52 (5), 995–1003.
Mohamed, M.A., et al., 2010. Brain metabolism and cognitive impairment in HIV infection: a 3-T magnetic resonance spectroscopy study. Magnetic Resonance Imaging 28 (9), 1251–1257.
Mulder, J., et al., 1994. Rapid and simple PCR assay for quantitation of human immunodeficiency virus type 1 RNA in plasma: application to acute retroviral infection. Journal of Clinical Microbiology 32 (2), 292–300.
Navia, B.A., Rostasy, K., 2005. The AIDS dementia complex: clinical and basic neuroscience with implications for novel molecular therapies. Neurotoxicity Research 8 (1–2), 3–24.
Navia, B.A., Jordan, B.D., Price, R.W., 1986a. The AIDS dementia complex: I. Clinical features. Annals of Neurology 19 (6), 517–524.
Navia, B.A., et al., 1986b. The AIDS dementia complex: II. Neuropathology. Annals of Neurology 19 (6), 525–535.
Negredo, E., et al., 2010. Nadir CD4 T cell count as predictor and high CD4 T cell intrinsic apoptosis as final mechanism of poor CD4 T cell recovery in virologically suppressed HIV-infected patients: clinical implications. Clinical infectious diseases: an official publication of the Infectious Diseases Society of America 50 (9), 1300–1308.
Nir, T.M., et al., 2013. Mapping white matter integrity in elderly people with HIV. Human Brain Mapping (http://dx.doi.org/10.1002/hbm.22228).
Palella Jr., F.J., et al., 1998. Declining morbidity and mortality among patients with advanced human immunodeficiency virus infection. HIV Outpatient Study Investigators. The New England Journal of Medicine 338 (3), 853–860.
Paley, M., et al., 1996. A multicenter proton magnetic resonance spectroscopy study of neurological complications of AIDS. AIDS Research and Human Retroviruses 12 (3), 213–222.
Patel, S.H., et al., 2003. Whole-brain N-acetylaspartate level and cognitive performance in HIV infection. AJNR. American Journal of Neuroradiology 24 (8), 1587–1591.
Paul, R., et al., 2002. Relationships between cognition and structural neuroimaging findings in adults with human immunodeficiency virus type-1. Neuroscience and Biobehavioral Reviews 26 (3), 353–359.
Paul, R.H., et al., 2008. Relative sensitivity of magnetic resonance spectroscopy and quantitative magnetic resonance imaging to cognitive function among nondemented individuals infected with HIV. Journal of the International Neuropsychological Society: JINS 14 (5), 725–733.
Pfefferbaum, A., et al., 2007. Diffusion tensor imaging with quantitative fibre tracking in HIV infection and alcoholism comorbidity: synergistic white matter damage. Brain: a journal of neurology 130 (Pt 1), 48–64.
Pfefferbaum, A., et al., 2009. Frontostriatal fiber bundle compromise in HIV infection without dementia. AIDS 23 (15), 1977–1985.
Price, R.W., Brew, B.J., 1988. The AIDS dementia complex. The Journal of Infectious Diseases 158 (5), 1079–1083.
Price, R.W., Brew, B.J., Rosenblum, M., 1990. The AIDS dementia complex and HIV-1 brain infection: a pathogenetic model of virus-immune interaction. Research Publications — Association for Research in Nervous and Mental Disease 68, 269–290.
Provencher, S.W., 1993. Estimation of metabolite concentrations from localized in vivo proton NMR spectra. Magnetic resonance in medicine: official journal of the Society of Magnetic Resonance in Medicine/Society of Magnetic Resonance in Medicine 30 (6), 672–679.
Provencher, S.W., 2001. Automatic quantitation of localized in vivo 1H spectra with LCModel. NMR in Biomedicine 14 (4), 260–264.
Ragin, A.B., et al., 2004. Whole brain diffusion tensor imaging in HIV-associated cognitive impairment. AJNR. American Journal of Neuroradiology 25 (2), 195–200.
Riddle, W.R., et al., 2004. Characterizing changes in MR images with color-coded Jacobians. Magnetic Resonance Imaging 22 (6), 769–777.
Rostasy, K., et al., 1999. Human immunodeficiency virus infection, inducible nitric oxide synthase expression, and microglial activation: pathogenetic relationship to the acquired immunodeficiency syndrome dementia complex. Annals of Neurology 46 (2), 207–216.
Sacktor, N., et al., 2005. A multicenter study of two magnetic resonance spectroscopy techniques in individuals with HIV dementia. Journal of Magnetic Resonance Imaging: JMRI 21 (4), 325–333.
Salvan, A.M., et al., 1997. Brain proton magnetic resonance spectroscopy in HIV-related encephalopathy: identification of evolving metabolic patterns in relation to dementia and therapy. AIDS Research and Human Retroviruses 13 (12), 1055–1066.
Schouten, J., et al., 2011. HIV-1 infection and cognitive impairment in the cART era: a review. AIDS 25 (5), 561–575.
Shen, D., Davatzikos, C., 2003. Very high-resolution morphometry using mass-preserving deformations and HAMMER elastic registration. NeuroImage 18 (1), 28–41.
Simioni, S., et al., 2010. Cognitive dysfunction in HIV patients despite long-standing suppression of viremia. AIDS 24 (9), 1243–1250.
Sled, J.G., Zijdenbos, A.P., Evans, A.C., 1998. A nonparametric method for automatic correction of intensity nonuniformity in MRI data. IEEE Transactions on Medical Imaging 17 (1), 87–97.
Studholme, C., et al., 2001. Detecting Spatially Consistent Structural Differences in Alzheimer's and Fronto Temporal Dementia Using Deformation Morphometry. MICCAI 41–48.
Tate, D.F., et al., 2009. Neuroimaging among HIV-infected patients: current knowledge and future directions. In: Tashima, K.T., et al. (Ed.), HIV and the Brain. Humana Press, New York, pp. 75–107.
Tate, D.F., et al., 2010. Quantitative diffusion tensor imaging tractography metrics are associated with cognitive performance among HIV-infected patients. Brain Imaging and Behavior 4 (1), 68–79.
Tate, D.F., et al., 2011. Regional areas and widths of the midsagittal corpus callosum among HIV-infected patients on stable antiretroviral therapies. Journal of Neurovirology 17 (4), 368–379.
Thompson, P.M., et al., 2000. Growth patterns in the developing brain detected by using continuum mechanical tensor maps. Nature 404 (6774), 190–193.
Thompson, P.M., et al., 2005. Thinning of the cerebral cortex visualized in HIV/AIDS reflects CD4+ T lymphocyte decline. Proceedings of the National Academy of Sciences of the United States of America 102 (43), 15647–15652.
Thompson, P.M., et al., 2006. 3D mapping of ventricular and corpus callosum abnormalities in HIV/AIDS. NeuroImage 31 (1), 12–23.

Toga, A.W., 1999. Brain Warping, 1st ed. Academic Press, San Diego.
Tracey, I., et al., 1996. Brain choline-containing compounds are elevated in HIV-positive patients before the onset of AIDS dementia complex: a proton magnetic resonance spectroscopic study. Neurology 46 (3), 783–788.
Tucker, K.A., et al., 2004. Neuroimaging in human immunodeficiency virus infection. Journal of Neuroimmunology 157 (1–2), 153–162.
Wang, Y., et al., 2010. Multivariate tensor-based morphometry on surfaces: application to mapping ventricular abnormalities in HIV/AIDS. NeuroImage 49 (3), 2141–2157.
Wu, Y., et al., 2006. Diffusion alterations in corpus callosum of patients with HIV. AJNR. American Journal of Neuroradiology 27 (3), 656–660.
Yiannoutsos, C.T., et al., 2004. Regional patterns of brain metabolites in AIDS dementia complex. NeuroImage 23 (3), 928–935.